ACS APPLIED MATERIALS & INTERFACES

Research Article

www.acsami.org

Amplified Thrombin Aptasensor Based on Alkaline Phosphatase and Hemin/G-Quadruplex-Catalyzed Oxidation of 1-Naphthol

Zhe-Han Yang, Ying Zhuo, Ruo Yuan,* and Ya-Qin Chai*

Key Laboratory of Luminescent and Real-Time Analytical Chemistry and Ministry of Education, College of Chemistry and Chemical Engineering, Southwest University, Chongqing 400715, P. R. China

ABSTRACT: An alkaline phosphatase (ALP)-based biosensor can in situ generate an electroactive product by enzymatic hydrolysis of inactive substrates. To obtain a higher signal-to-background ratio, a chemical redox cycling signal-amplified strategy based on the addition of a strong reducing agent has often be applied in the construction of ALP-based biosensors. However, the strong reducing agent not only affects the activity of ALP but also readily reacts with dissolved oxygen, leading to inaccurate results. In this work, a new signal-amplified strategy for a thrombin (TB) aptasensor based on the catalytic oxidation of ALP-generated products, 1-naphthol (NP), using hemin/G-quadruplex DNAzymes was reported. We implemented gold-nanoparticle-decorated zinc oxide nanoflowers (Au-ZnO) as the matrix for immobilizing ALP and TB aptamer (TBA) and then labeled it with hemin to form hemin/G-quadruplex/ALP/Au-ZnO bioconjugates (TBA II bioconjugates). Through a "sandwich" reaction, TBA II bioconjugates were captured on the electrode surface. The amplified signal was carried out in two steps: (i) an ALP-catalyzed inactive substrate, 1-naphthyl phosphate (NPP), in situ produces NP on the surface of the electrode; (ii) on the one hand, NP as a new reactant could be directly electrooxidized and generated an electrochemical signal, but, on the other hand, NP could be oxidized by hemin/G-quadruplex in the presence of H_2O_2, resulting in amplification of the electrochemical signal. The proposed TB aptasensor achieved a linear range of 1 pM to 30 nM with a detection limit of 0.37 pM (defined as S/N = 3).

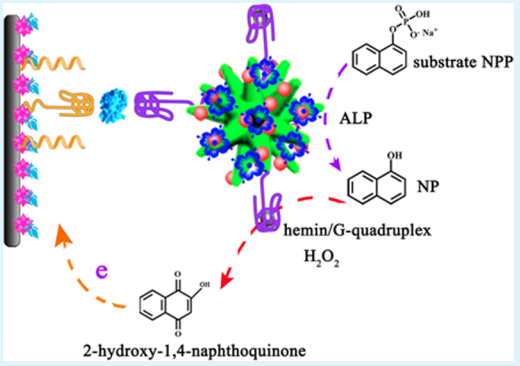

KEYWORDS: *alkaline phosphatase, hemin/G-quadruplex, signal-amplified aptasensor, catalytic oxidation of 1-naphthol*

1. INTRODUCTION

Detectable signal amplification is expected to increase the detection sensitivity of a biosensor.[1,2] As a result, a variety of strategies for signal amplification have been explored including the use of nanomaterials,[3,4] rolling circle amplification,[5−7] hybridization chain reaction,[8,9] etc. Alternatively, enzyme-catalyzed signal amplification[10,11] has been widely used in the construction of a biosensor because of its specificity and high catalytic efficiency. Among various enzymes, alkaline phosphatase (ALP) has attained a great deal of attention because it can in situ generate electroactive products by enzymatic hydrolysis of inactive substrates, including L-ascorbic acid 2-phosphate,[12,13] 4-aminophenyl phosphate,[14] 4-amino-1-naphthyl phosphate,[15] and 1-naphthyl phosphate (NPP).[16] On the base of this property, many ALP-based biosensors have been explored for DNA,[17] mircoRNA,[18] and protein[19] detection. To obtain a higher signal-to-background ratio, chemical redox cycling signal-amplified strategies are applied in the construction of ALP-based biosensors, wherein the ALP-generated products are electrooxidized on the surface electrode and then reduced by a strong reducing agent.[20,21] However, the strong reducing agent not only affects the activity of ALP but also readily reacts with dissolved oxygen, leading to inaccurate results. A new signal-amplified strategy based on the catalytic oxidation of ALP-generated products using nanomaterials or enzymes can be used to overcome this disadvantage. In our previous work, we used graphene oxide and platinum-nanoparticle-functionalized CeO_2 nanocomposites (Pt/CeO_2/GO) as oxidation agents for the catalytic oxidation of 1-naphthol (NP), an ALP-generated product, to construct a signal-amplified immunosensor.[22] To our knowledge, there are few reports focused on the catalytic oxidation of ALP-generated products for signal amplification, which may be ascribed to the fact that few nanomaterials or enzymes could be used for the oxidation of ALP-generated products.

Hemin/G-quadruplex DNAzymes, the complexation of hemin with a guanine-rich single-stranded nucleic acid, were applied most frequently over the past decade in the construction of an electrochemical biosensor,[23,24] because they were found to mimic the biocatalytic functions of different natural enzymes. For example, hemin/G-quadruplex mimics the biocatalytic activities of NADH oxidase and NADH peroxidase, where it catalyzes the oxidation of NADH to NAD^+ under aerobic conditions and in the existent of H_2O_2, respectively.[25] Also, it was found to mimic different enzymatic activities of horseradish peroxidase, including the electrocatalyzed reduction

Received: February 2, 2015
Accepted: April 24, 2015
Published: April 24, 2015

DOI: 10.1021/acsami.5b00988
ACS Appl. Mater. Interfaces 2015, 7, 10308−10315

Scheme 1. Schematic Illustration of ALP and Hemin/G-Quadruplex as Catalysts for an in Situ Amplified Electrochemical Detection Signal

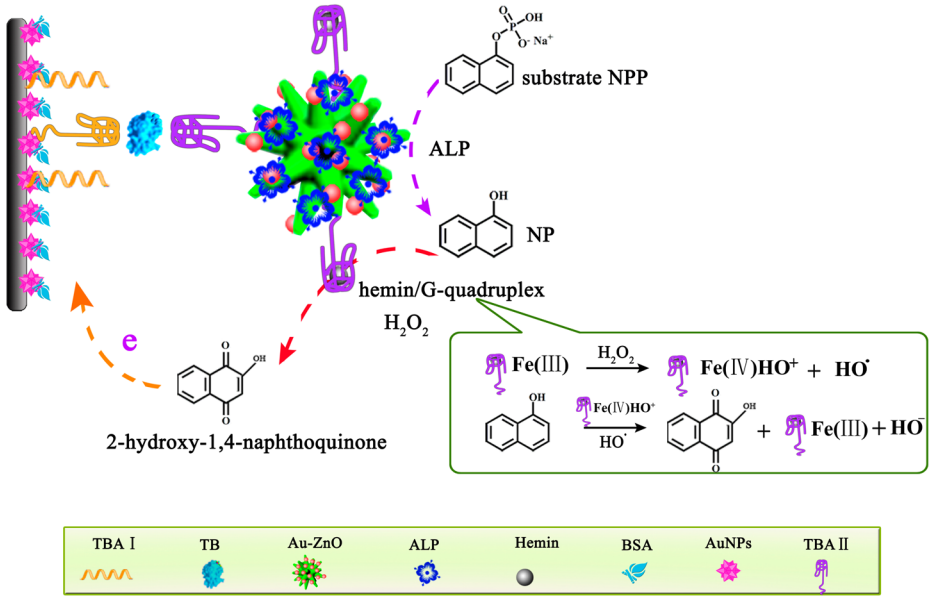

of H_2O_2[26] and the catalyzed aerobic oxidation of thiols to disulfides in the presence of H_2O_2.[27] Furthermore, the nucleic acid sequences of hemin/G-quadruplex can directly act as recognition elements for genes, aptamer−substrate complexes, and metal ions.[28] Therefore, various amplified biosensors based on hemin/G-quadruplex have been reported for DNA, protein, and metal-ion detection.[29−31]

In this work, we described novel catalytic activity of the hemin/G-quadruplex for the catalytic oxidation of NP in the presence of H_2O_2. Inspired by this, an amplified aptasensor was constructed based on an in situ producing electroactive NP by catalysis of ALP and hemin/G-quadruplex as a catalytic amplifier for sensitive thrombin (TB) detection. First, we implemented gold-nanoparticle (AuNP)-decorated zinc oxide nanoflowers (Au-ZnO) as the matrix for immobilizing ALP and TB aptamer (TBA) (TBA/ALP/Au-ZnO). The obtained TBA/ALP/Au-ZnO was then labeled with hemin to form hemin/G-quadruplex/ALP/Au-ZnO bioconjugates (TBA II bioconjugates). ZnO nanoflowers, as a semiconductor nanomaterial, possess superior properties such as lower cost, nontoxicity, large surface area, and high chemical stability.[32−34] After AuNP decoration, electronic conduction of ZnO nanoflowers will be improved. Moreover, amounts of ALP and TBA could be readily immobilized on Au-ZnO through chemical absorption between AuNPs and $-NH_2$ of ALP and TBA. Through a "sandwich" reaction, TBA II bioconjugates were captured on the electrode surface, but almost no electrochemical signal was carried out. After the addition of NPP, an ALP substrate, ALP catalyzed inactive NPP to in situ produce NP on the surface of the electrode. On the one hand, NP as a new reactant could be directly electrooxidized and generated an electrochemical signal. On the other hand, NP could be oxidized by hemin/G-quadruplex in the presence of H_2O_2, resulting in amplification of the electrochemical signal.

2. EXPERIMENTAL SECTION

2.1. Chemicals and Materials. Hemin, alkaline phosphatase (ALP; buffered aqueous glycerol solution, ≥6500 DEA units/mg of protein), thrombin (TB), bovine serum albumin (BSA), and gold chloride ($HAuCl_4$) were obtained from Sigma-Aldrich Chemical Co. (St. Louis, MO). Thrombin aptamers 5′-NH_2-(CH_2)6-GGTTGGTGTGGTTGG-3′ (TBA I) and 5′-NH_2-AGTCCGTGG-TAGGGCAGGTTGGGGTGACT-3′ (TBA II) were purchased from Sangon Biotech (Shanghai) Co., Ltd. $Zn(NO_3)_2{\cdot}6H_2O$, NaOH, and methanol were from Ke Long Bio. Co. Ltd. (Chengdu, China). Tris buffer (pH 7.4) containing 140 mM NaCl, 5 mM KCl, 2 mM ethylenediaminetetraacetic acid, and 1 mM $MgCl_2$ was used as the binding buffer solution. 0.1 M phosphate buffered saline (PBS; pH 7.5) was prepared as the working buffer solution using 0.1 M Na_2HPO_4, 0.1 M NaH_2PO_4, and 2 mM $MgCl_2$. All other chemicals were of reagent grade and were used as received. Doubly distilled water was used throughout the study.

2.2. Apparatus and Measurements. The morphologies and structures of the samples were characterized with scanning electron microscopy (SEM; S-4800, Hitachi, Japan) and transmission electron microscopy (TEM; H600, Hitachi, Japan). Raman measurements were conducted with a Renishaw 2400 laser Raman microscope equipped with a 532 nm argon-ion laser of 2 μm spot size for excitation (Renishaw, U.K.). Ultraviolet−visible (UV−vis) spectra were performed by a UV-2501 PC spectrometer (Shimadzu, Japan). X-ray photoelectron spectroscopy (XPS) measurements were carried out using a VG Scientific ESCALAB 250 spectrometer (Thermoelectricity Instruments, USA) and using Al Ka X-ray (1486.6 eV) as the light source. A conventional three-compartment electrochemical cell, comprising a platinum wire auxiliary electrode, a modified 4-mm-diameter glassy carbon electrode (GCE), and a saturated calomel reference electrode, was used. Cyclic voltammetry (CV) and differential pulse voltammetry (DPV) were recorded with a CHI 1040C electrochemical workstation (Shanghai Chenhua Instrument, China).

2.3. Preparation of ZnO Nanoflowers and Au-ZnO Nanocomposites. ZnO nanoflowers were synthesized according to a previously reported method with a little modification.[35] Briefly, 10 mL of a $Zn(NO_3)_2{\cdot}6H_2O$ (0.5 M) aqueous solution was added to 10 mL of a NaOH (4 M) aqueous solution drop by drop under stirring. Then the mixture solution was stirred at room temperature for 12 h. After that, the obtained ZnO nanoflower solution was washed with doubly distilled water and ethanol several times. Finally, the ZnO nanoflowers were dried at 60 °C.

The Au-ZnO nanocomposites were performed by a hydrothermal method with some modifications.[36] First, 2 mL of $HAuCl_4$ (1% w/w) and 0.5 mL of methanol (99.5% v/v) were added to 10 mL of doubly

DOI: 10.1021/acsami.5b00988
ACS Appl. Mater. Interfaces 2015, 7, 10308−10315

distilled water. The pH of the solution was adjusted to 7−8 with 0.01 M NaOH under stirring. Next, 15 mg of the as-obtained ZnO nanoflowers was added to the solution and stirred for about 1 h. Then the solution was transferred to a 30 mL Teflon-lined stainless steel autoclave and maintained at 120 °C for 1 h. After being cooled to room temperature, the obtained Au-ZnO nanocomposites were collected by centrifugation, washed with doubly distilled water and ethanol, and then dried at 60 °C in air.

2.4. Preparation of TBA II Bioconjugates. First, the prepared Au-ZnO nanocomposites (10 mg) were dissolved into 2 mL of PBS (pH 7.5). Second, 100 μL of ALP (1.0 mg/mL, ≥6500 DEA units/mg) and 200 μL of TBA (0.25 μM) were added into a Au-ZnO nanocomposites solution and stirred for 12 h under 4 °C. As a result, amounts of ALP and TBA were immobilized onto the Au-ZnO bionanocomposite (TBA/ALP/Au-ZnO) through interaction between AuNPs and $-NH_2$ in ALP and TBA. Then, 100 μL of a hemin (2 mg/mL) solution was introduced to the TBA/ALP/Au-ZnO bionanocomposite via formation of a hemin/G-quadruplex structure. Finally, 100 μL of ALP was added to the solution to block the remaining active sites with 2 h stirring. TBA II bioconjugate was obtained by centrifuging and washing with Tris buffer, and it was stored at 4 °C when not in use.

2.5. Fabrication Process of the Sandwich-Type Electrochemical Aptasensor. The fabrication process of the sandwich-type aptasensor is illustrated in Scheme 1. Prior to use, the GCE was carefully polished with 0.3 and 0.05 μm alumina powder to a mirrorlike surface. After that, the GCE was sonicated in doubly distilled water and rinsed thoroughly. To introduce the AuNP layer (dep-Au), the cleaned GCE was immediately soaked in a $HAuCl_4$ solution (1% w/w) and electrodeposited at −0.2 V for 30 s. Then, NH_2-terminated thrombin aptamer (TBA I) immobilized on the electrode surface by Au-NH_2 after 16 h of incubation at room temperature. In addition, the modified electrode was incubated with a BSA solution (15 μL, 1% w/w) for 1 h to block the remaining active sites. Subsequently, a TB (15 μL) standard solution with different concentrations was incubated on the resulting electrode surface for 50 min at room temperature. At last, 15 μL of TBA II bioconjugates was dropped onto the electrode surface for 1 h, and the proposed aptasensor was obtained for electrochemical measurement.

3. RESULTS AND DISCUSSION

3.1. Characterizations of ZnO Nanoflowers and Au-ZnO Nanocomposites. The morphologies of ZnO nanoflowers and Au-ZnO nanocomposites were characterized by SEM and TEM. As shown in Figure 1A,C, ZnO is mainly composed of hierarchical flowerlike structures, which have an array of oriented tapered branches with approximately 1−2 μm length. The close-up SEM image shown in Figure 1E reveals that the petal had a very smooth surface. When $HAuCl_4$ was introduced and reduced, some highlights could be observed on the surface of ZnO nanoflowers, as shown in Figure 1B,D, indicating that the AuNPs were successfully reduced on the surface of the ZnO nanoflowers. The TEM micrograph of Au-ZnO nanocomposites is shown in Figure 1F. AuNPs exhibiting a dark contrast could be found to be deposited onto the smooth and crystalline surface of ZnO nanoflowers, which also confirm that AuNPs were loaded onto ZnO nanoflowers.

The UV−vis absorption and Raman spectra of ZnO nanoflowers and Au-ZnO nanocomposites are shown in Figure 2. As seen from Figure 2A, the bare ZnO nanoflowers showed a strong adsorption peak centered at about 350 nm and did not show any absorption between 400 and 800 nm (curve a). However, the Au-ZnO nanocomposites displayed an obvious absorption with a maximum absorption wavelength of 532 nm (curve b), which was ascribed to the localized surface plasmon resonance of AuNPs, indicating that the sample of Au-ZnO nanocomposites consisted of ZnO and AuNPs. Figure 2B

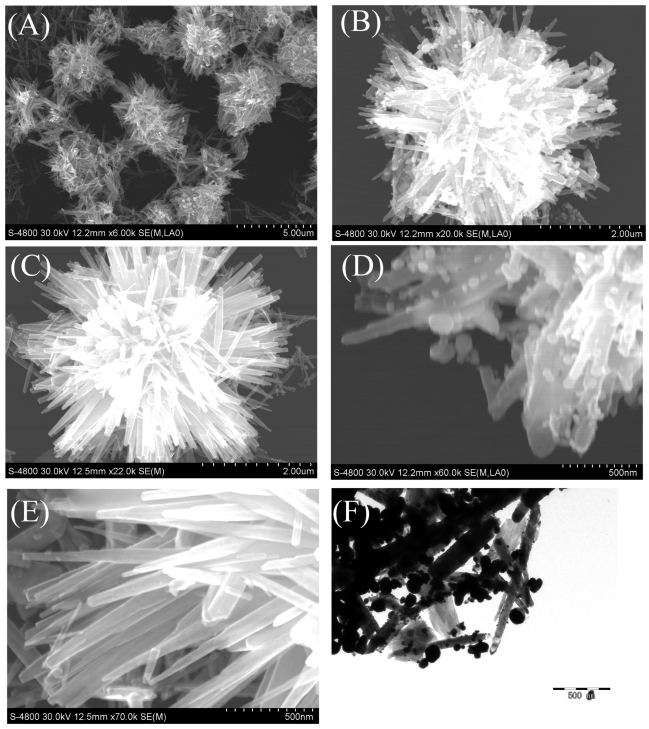

Figure 1. SEM images of ZnO nanoflowers (A, C, and E) and Au-ZnO nanocomposites (B and D) at different magnifications. TEM image of Au-ZnO nanocomposites (F).

shows the Raman spectra of ZnO nanoflowers and Au-ZnO nanocomposites excited at 532 nm with 10% laser power. As seen from curve a, Raman signals of ZnO nanoflowers were observed at 300, 589, 791, 1104, an 1748 cm^{-1}. For Au-ZnO nanocomposites, stronger Raman signals were achieved in comparison with ZnO nanoflowers (curve b). This increase of the Raman intensity was attributed to the attachment of AuNPs on the surface of ZnO nanoflowers. These experimental results further identified that ZnO nanoflowers and Au-ZnO nanocomposites were successfully prepared.

3.2. XPS Characterization of TBA II Bioconjugates. XPS is a powerful technique that allows estimation of the elemental and chemical composition of a bionanocomposite. Therefore, XPS characterization was employed in this study for the investigation of elemental analysis of TBA II bioconjugates. As seen from Figure 3A, the fully scanned spectra demonstrated the existence of nitrogen, gold, zinc, and iron elements in TBA II bioconjugates. The peak at 395.33 eV could be assigned to N 1s (Figure 3 B), which mainly derived from the ALP. The Au 4f core level (89.38 eV; Figure 3C) and the Zn 2p doublet (1022.22 and 1044.23 eV; Figure 3 D) confirmed the presence of Au-ZnO. Figure 3E represents the XPS signature of the Fe 2p (710.08 eV; Figure 3 E) for the resulting hemin.

3.3. CV Behavior of the Aptasensor. In order to characterize the modified process of the sensing surface, CV experiment was used to record the behavior of the proposed aptasensor. As shown in Figure 4A, the probe of the $[Fe(CN)_6]^{3-/4-}$ showed a well-defined redox peak on bare GCE (curve a). When AuNPs were deposited on the bare GCE, AuNPs/GCE showed an increase in the redox peak, which was attributed to the superior conductivity ability of the AuNPs (curve b). After TBA I bioconjugates were combined covalently on AuNPs/GCE, the peak current dramatically decreased, suggesting the successful immobilization of TBA I

DOI: 10.1021/acsami.5b00988
ACS Appl. Mater. Interfaces 2015, 7, 10308−10315

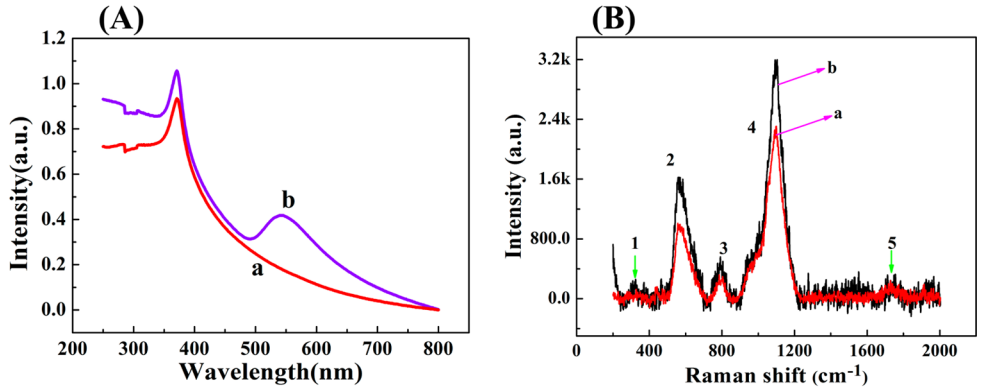

Figure 2. (A) UV−vis absorption spectra of ZnO nanoflowers (a) and Au-ZnO nanocomposites (b). (B) Raman spectra of ZnO nanoflowers (a) and Au-ZnO nanocomposites (b).

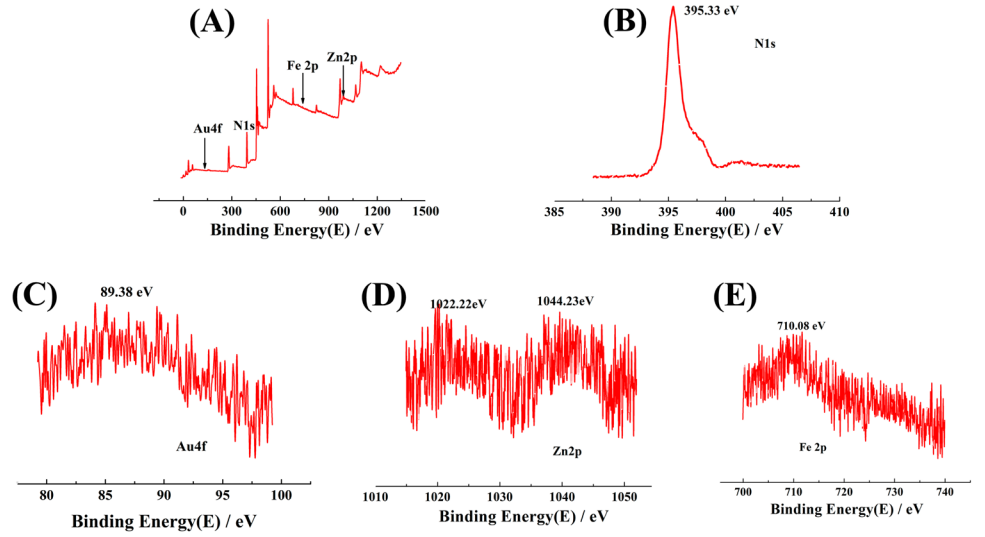

Figure 3. XPS analyses for (A) the full region of XPS for TBA II bioconjugates, (B) the N 1s region, (C) the Au 4f region, (D) the Zn 2p region, and (E) the Fe 2p region.

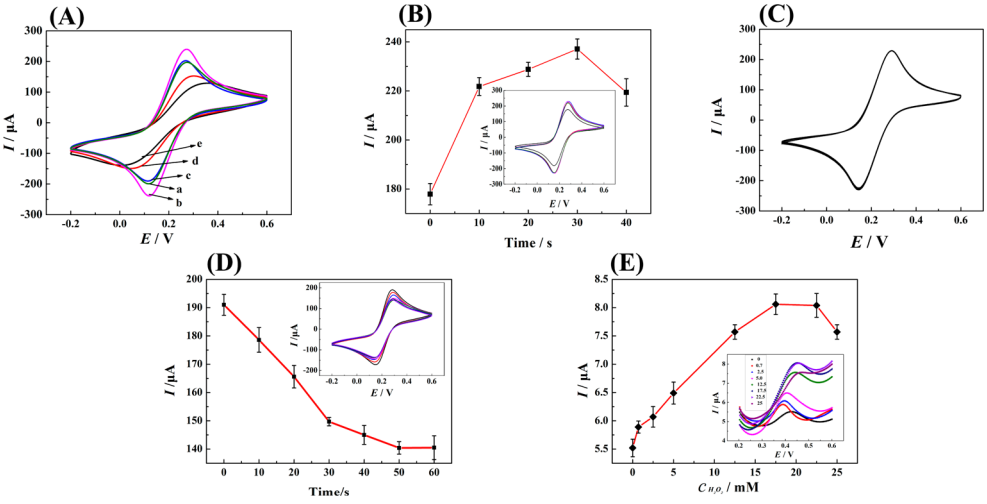

Figure 4. (A) CV responses of different modified electrodes in pH 7.4 PBS containing 5.0 mM $[Fe(CN)_6]^{3-/4-}$ as the redox probe at a scan rate of 50 mV/s: (a) bare GCE; (b) AuNP/GCE; (c) TBA I/AuNP/GCE; (d) BSA/TBA I/AuNP/GCE; (e) TB/BSA/TBA I/AuNP/GCE. Optimization of the experimental parameters: (B) Effect of the AuNP electrodepositing time on the electrochemical response. The inset shows the different current peaks at each electrodepositing time. (C) Stability of the AuNP modified electrode under successive CV scans for 30 cycles. (D) Influence of the incubation time of TB on the signal response of the aptasensor. The inset shows the different current peaks at each incubation time. (E) Effect of the concentrations of H_2O_2 on signal amplification. The inset shows the different DPV responses at each concentration of H_2O_2.

DOI: 10.1021/acsami.5b00988
ACS Appl. Mater. Interfaces 2015, 7, 10308−10315

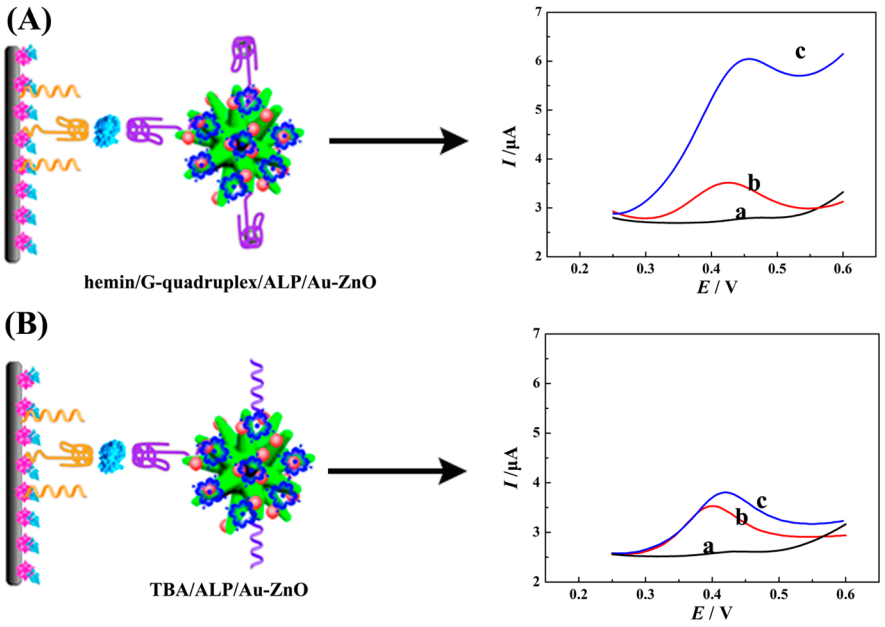

Figure 5. (A and B) DPV of the modified electrode using hemin/G-quadruplex/ALP/Au-ZnO and TBA/ALP/Au-ZnO as tracers in the absence of NPP (a), in the presence of 37.5 mg/mL NPP (b), and in the presence of 37.5 mg/mL NPP with 17.5 mM H_2O_2 (c).

on the surface of AuNPs/GCE (curve c). The peak current also decreased after binding with BSA (curve d). After incubation with TB, the peak current further decreased, accounting for the successful specific binding between TB and TBA I, which retard the electron-transfer tunnel (curve e).

3.4. Optimization of the Experimental Parameters: Electrodepositing Time of AuNPs, Incubation Time of TB, and Concentration of H_2O_2. The electrodepositing time of AuNPs was an important parameter in the construction an electrochemical aptasensor because the preparation of thin AuNP films with a high density of AuNPs was often desired for electronics transfer. Figure 2B showed the effect of the different electrodepositing times of AuNPs on the CV response in 5 mM $[Fe(CN)_6]^{3-/4-}$. The current change increased with the increment of the electrodepositing time; the maximum current was achieved at 30 s and then decreased. The result might be ascribed to the fact that a longer electrodeposition time resulted in the formation of overdense nanoparticulate films, which was not conducive to electronics transfer. Therefore, 30 s was selected as the optimum electrodepositing time for aptasensor construction. In addition, to investigate the stability of the electrodeposited AuNPs, a CV experiment was used to evaluate the behavior of the AuNP modified electrode at 5 mM $[Fe(CN)6]^{3-/4-}$. As shown in Figure 4C, the response current decreased only about 1.3% of its initial response after scanning 30 circles for continuous CV measurement, indicating that the stability of the electrodeposited AuNPs was acceptable.

Besides, the incubation time for the reaction between TB and TBA greatly affected the amperometric response for TB assay. The experiments were carried out at room temperature, and the CV response was recorded in 5 mM $[Fe(CN)_6]^{3-/4-}$ with different incubation times. As shown in Figure 4D, after 10 nM TB incubation with TBA I, a decrease in the response current was obtained because TB is a kind of protein that hinders electron transport between the solution and electrode. Also, the amperometric response decreased with the increment of the incubation time and leveled off after 50 min. Longer incubation time did not improve the response. Therefore, 50 min was chosen as the incubation time for the determination of TB in the following experiments.

Furthermore, the effect of the H_2O_2 concentration on the electrocatalytic activity was investigated (Figure 4E). After incubation with 10 nM TB, the proposed aptasensor was conducted by using DPV measurement in PBS (pH 7.5) with seven H_2O_2 concentrations (0.7, 2.5, 5.0, 12.5, 17.5, 22.5, and 25.0 mM). The oxidation peak current increased rapidly with an increase in the concentration of H_2O_2 and then tended to level off after more than 17.5 mM. The response current decreased when PBS containing 25.0 mM H_2O_2. Thus, the optimal concentration of H_2O_2 was 17.5 mM, which was adopted in the subsequent work.

3.5. Catalytic Activity Test. To demonstrate the feasibility of this approach and the potential of hemin/G-quadruplex for electrochemical signal amplification, DPV experiments were conducted to record the experimental result. As shown in Figure 5A, no oxidation peaks were observed in the DPV of the modified electrode in the absence of a NPP substrate (curve a). After NPP was added into the buffer, a well-defined oxidation peak current was observed (curve b) that was ascribed to electrooxidation of the enzymatically generated NP, a common hydrolytic product of ALP. Then, H_2O_2 was added into the buffer, and considerable enhancement of the oxidation current was observed (curve c). Here, to confirm this enhancement induced by hemin/G-quadruplex, the contrast probe TBA/ALP/Au-ZnO was prepared. The same batch of aptasensors was incubated with 0.5 nM TB and then with TBA/ALP/Au-ZnO and hemin/G-quadruplex/ALP/Au-ZnO solutions respectively and conducted under the same conditions. As shown in Figure 5B, after 17.5 mM H_2O_2 was added, the DPV response current of the aptasensor with TBA/ALP/Au-ZnO increased in comparison to that in the absence of H_2O_2, which may be ascribed to the fact that NP was directly oxidized by H_2O_2. However, the current enhancement of the aptasensor with hemin/G-quadruplex/ALP/Au-ZnO was much higher than that of the aptasensor with TBA/ALP/Au-ZnO in the presence of H_2O_2, indicating that the current enhancement was

DOI: 10.1021/acsami.5b00988
ACS Appl. Mater. Interfaces 2015, 7, 10308−10315

Scheme 2. Possible Mechanism of Hemin/G-Quadruplex for NP

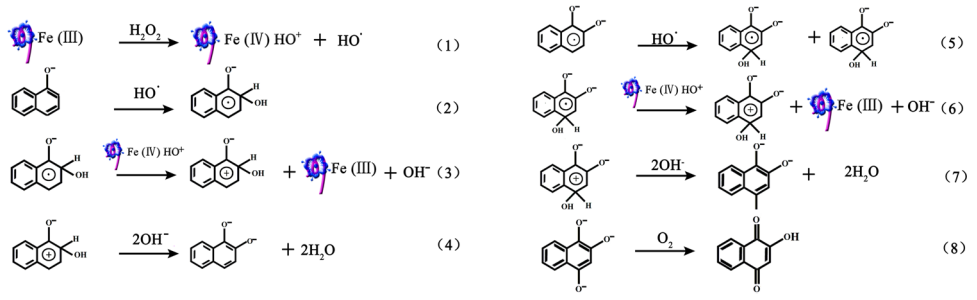

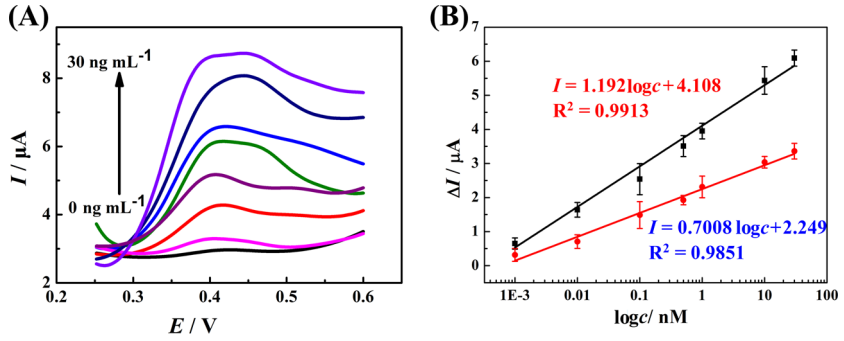

Figure 6. (A) DPV response of the proposed aptasensor after incubation with different concentrations of TB. (B) Calibration curve of the intensity current after subtraction of the background current of the aptasensor with hemin/G-quadruplex/ALP/Au-ZnO (red line) and TBA/ALP/Au-ZnO (blue line) for 1 pM to 30 nM in the presence of H_2O_2.

mainly caused by hemin/G-quadruplex catalytic oxidation of NP rather than H_2O_2. This confirmed the catalytic activity of hemin/G-quadruplex for NP and demonstrated promising characteristics in signal amplification. The current enhancement demonstrated the conceptual validity of this strategy for achieving high detection sensitivity of TB. The possible mechanism of hemin/G-quadruplex as a catalyst for NP is shown in Scheme 2.[37]

3.6. Electrochemical Response to TB. Under optimized conditions, DPV measurement was employed to detect TB using hemin/G-quadruplex/TBA/ALP/Au-ZnO as the tracer. The proposed aptasensor was incubated with a series of TB standard solutions with various concentrations. As seen from Figure 6 A, the DPV response increased with the increment of the TB concentration according to the typical sandwich mechanism. Besides, a quite low DPV current response was observed in the presence of 0 nM TB, indicating negligible unspecific binding. As a result, the increase of the oxidation current was proportional to the TB concentration in a linear range of 1 pM to 30 nM, and the linear equation was I = 1.192 log c + 4.108 (R^2 = 0.9913) with a detection limit of 0.37 pM (defined as S/N = 3; Figure 6B, red line). For comparison, the current response of the aptasensor with TBA/ALP/Au-ZnO was also recorded, and the regression equation was I = 0.7008 log c + 2.249 (R^2 = 0.9851) (Figure 6B, blue line). The higher sensitivity of the proposed aptasensor may be ascribed to significant amplification of the hemin/G-quadruplex biocatalytic system.

3.7. Specificity, Reproducibility, and Stability of the Aptasensor. To assess the specificity of the proposed aptasensor, some other proteins such as carbohydrate antigen 19-9 (CA 19-9), carcinoembryonic antigen (CEA), and BSA as possible interferences were examined under the same experimental conditions. As shown in Figure 7, no significant

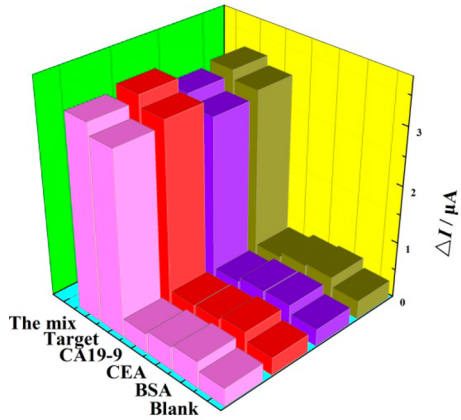

Figure 7. Specificity of the electrochemical aptasensor (10 nM TB was used in this case).

change of the current response could be observed in the detection of CA 19-9 (200 nM), CEA (200 nM), and BSA (200 nM) in comparison with the blank test. On the contrary, a high current response was obtained after incubation with the target TB (10 nM). Meanwhile, when 10 nM TB coexisted with the above three interferences (200 nM), no apparent signal change existed in the buffer, compared with the case of only TB. The results demonstrated the high specificity of the proposed aptasensor for TB detection.

The reproducibility of this system was evaluated by intra- and interassay coefficients of variation. The interassay of the proposed aptasensor was evaluated by the following method: Four of the proposed aptasensors were incubated with 10 nM TB and detected under the same experimental conditions. The aptasensors exhibited similar electrochemical signals with a relative standard deviation (RSD) of 12.1%. In addition, the

DOI: 10.1021/acsami.5b00988
ACS Appl. Mater. Interfaces 2015, 7, 10308−10315

intraassay of the proposed aptasensor was investigated by detecting the same proposed aptasensor five times, and a RSD of 9.9% was obtained. The results illustrated the acceptable reproducibility of the proposed aptasensor. Besides, the stability of the proposed aptasensor was demonstrated by a long-term storage assay. Five aptasensors were evaluated intermittently (every 4 days) by DPV measurement and stored at 4 °C when not use. After 16 days, the electrochemical signal retained 91.5 ± 0.2%, 93.2 ± 0.1%, 94.1 ± 0.3%, 90.1 ± 0.1%, and 92.7 ± 0.1% of its initial current, which indicated that the aptasensor had good stability.

3.8. Detection of TB in Clinical Serum Samples and Evaluation of the Method Trueness. In order to assess the feasibility of the newly developed aptasensor for TB detection, the practical applicability was investigated by adding different concentrations of TB into healthy human real serum samples obtained from the DaPing Hospital (Chongqing, China). Briefly, 1 mL healthy human serum samples were diluted with 0.1 M PBS (pH 7.0) to reach a final volume of 10 mL. Then, aptasensor with incubation of the serum samples was investigated to assess the effect of the prepared serum samples for the TB aptasensor. Compared to the blank test in PBS, no significant change of the current response could be observed, indicating almost no TB in the serum samples. After that, different concentrations of TB solution were prepared with the diluted serum samples. Experimental results are described in Table 1, with the recovery was ranging from 94% to 110% and RSDs varying from 2.30% to 5.23%. The results demonstrated excellent promise for the detection of TB in real biological samples.

Table 1. Recovery Results of the Proposed Aptasensor in Human Serum

sample no.	added (nM)	found (nM)	recovery (%)	RSD (%)
1	1.0×10^{-1}	9.4×10^{-2}	94	1.3
2	1.0	1.1	110	4.56
3	5.0	5.2	104	2.89
4	10	9.4	94	5.46
5	15	15.3	102	3.21

4. CONCLUSIONS

In summary, the present study demonstrated novel catalytic activity of the hemin/G-quadruplex DNAzyme for oxidation of NP in the presence of H_2O_2. On the basis of this property, we have developed a signal amplification aptasensor by combining ALP and hemin/G-quadruplex DNAzyme. The detection signal of the aptasensor output involved two steps: (i) ALP-catalyzed NPP hydrolysis to produce NP; (ii) NP then oxidized by hemin/G-quadruplex in the presence of H_2O_2. These two catalytic processes resulted in amplification of the electrochemical signal. More importantly, the advantages of the hemin/G-quadruplex system rest on the fact that many aptamers could yield G-quadruplex/substrate complexes. Thus, a biosensor based on this new catalytic activity of hemin/G-quadruplex could be developed using different aptamers or G-rich sequences for the sensitive detection of protein, DNA, or metal ions.

AUTHOR INFORMATION

Corresponding Authors

*Tel.: +86-23-68252277. Fax: +86-23-68253172. E-mail: yuanruo@swu.edu.cn.

*Tel.: +86-23-68252277. Fax: +86-23-68253172. E-mail: yqchai@swu.edu.cn.

Notes

The authors declare no competing financial interest.

ACKNOWLEDGMENTS

The authors are grateful for the National Natural Science Foundation of China (Grants 21275119 and 51473136) and the Fundamental Research Funds for the Central Universities, China (Grants XDJK2013A027 and XDJK2014A012).

REFERENCES

(1) Shih, P. M.; Liu, T. K.; Tan, K. T. Fluorescence Amplified Detection of Proteases by the Catalytic Activation of a Semisynthetic Sensor. *Chem. Commun.* **2013**, *49*, 6212−6214.

(2) He, P.; Liu, L.; Qiao, W.; Zhang, S. Ultrasensitive Detection of Thrombin Using Surface Plasmon Resonance and Quartz Crystal Micro Balance Sensors by Aptamer-based Rolling Circle Amplification and Nanoparticle Signal Enhancement. *Chem. Commun.* **2014**, *50*, 1481−1484.

(3) Lei, J.; Ju, H. Signal Amplification using Functional Nanomaterials for Biosensing. *Chem. Soc. Rev.* **2012**, *41*, 2122−2134.

(4) Liu, X.; Aizen, R.; Freeman, R.; Yehezkeli, O.; Willner, I. Multiplexed Aptasensors and Amplified DNA Sensors Using Functionalized Graphene Oxide: Application for Logic Gate Operations. *ACS Nano* **2012**, *6*, 3553−3563.

(5) Ji, H.; Yan, F.; Lei, J.; Ju, H. Ultrasensitive Electrochemical Detection of Nucleic Acids by Template Enhanced Hybridization Followed with Rolling Circle Amplification. *Anal. Chem.* **2012**, *84*, 7166−717.

(6) Li, J.; Deng, T.; Chu, X.; Yang, R.; Jiang, J.; Shen, G.; Yu, R. Signal Enhancement Strategy for a Micro-arrayed Polydiacetylene (PDA) Immunosensor using Enzyme-catalyzed Precipitation. *Anal. Chem.* **2010**, *82*, 2811−2816.

(7) Wen, Y.; Xu, Y.; Mao, X.; Wei, Y.; Song, H.; Chen, N.; Huang, Q.; Fan, C.; Li, D. DNAzyme-Based Rolling-Circle Amplification DNA Machine for Ultrasensitive Analysis of MicroRNA in Drosophila Larva. *Anal. Chem.* **2012**, *84*, 7664−7669.

(8) Huang, J.; Wu, Y.; Chen, Y.; Zhu, Z.; Yang, X.; Yang, C. J.; Wang, K.; Tan, W. Pyrene-Excimer Probes Based on the Hybridization Chain Reaction for the Detection of Nucleic Acids in Complex Biological Fluids. *Angew. Chem., Int. Ed.* **2011**, *50*, 401−404.

(9) Xuan, F.; Hsing, I. M. Triggering Hairpin-Free Chain-Branching Growth of Fluorescent DNA Dendrimers for Nonlinear Hybridization Chain Reaction. *J. Am. Chem. Soc.* **2014**, *136*, 9810−9813.

(10) Lee, J. U.; Jeong, J. H.; Lee, D. S.; Sim, S. J. Signal Enhancement Strategy for a Micro-arrayed Polydiacetylene (PDA) Immunosensor using Enzyme-catalyzed Precipitation. *Biosens. Bioelectron.* **2014**, *61*, 314−320.

(11) Du, D.; Zou, Z.; Shin, Y.; Wang, J.; Wu, H.; Engelhard, M. H.; Liu, J.; Aksay, I. A.; Lin, Y. Sensitive Immunosensor for Cancer Biomarker Based on Dual Signal Amplification Strategy of Graphene Sheets and Multienzyme Functionalized Carbon Nanospheres. *Anal. Chem.* **2010**, *82*, 2989−2995.

(12) Nassef, H. M.; Redondo, M. C. B.; Ciclitira, P. J.; Ellis, H. J.; Fragoso, A.; Sullivan, C. K. Electrochemical Immunosensor for Detection of Celiac Disease Toxic Gliadin in Food stuff. *Anal. Chem.* **2008**, *80*, 9265−9271.

(13) Gao, Z.; Deng, K.; Wang, X. D.; Miró, M.; Tang, D. High-Resolution Colorimetric Assay for Rapid Visual Readout of Phosphatase Activity Based on Gold/Silver Core/Shell Nanorod. *ACS Appl. Mater. Interfaces* **2014**, *6*, 18243−18250.

DOI: 10.1021/acsami.5b00988
ACS Appl. Mater. Interfaces 2015, 7, 10308−10315

(14) Pembertona, R. M.; Hart, J. P.; Stoddarda, P.; Foulkes, J. A. A Comparison of 1-Naphthyl Phosphate and 4-Aminophenyl Phosphate as Enzyme Substrates for Use with a Screen-printed Amperometric Immunosensor for Progesterone in Cows' Milk. *Biosens. Bioelectron.* **1999**, *5*, 495−503.
(15) Zhou, Y.; Li, B.; Wang, M.; Yang, Z.; Yin, H.; Ai, S. Enzyme-based Electrochemical Biosensor for Sensitive Detection of DNA Demethylation and the Activity of DNA Demethylase. *Anal. Chim. Acta* **2014**, *840*, 28−32.
(16) Prieto-Simó, B.; Saint, C.; Voelcker, N. H. Electrochemical Biosensors Featuring Oriented Antibody Immobilization via Electrografted and Self-Assembled Hydrazide Chemistry. *Anal. Chem.* **2014**, *86*, 1422−1429.
(17) Kaatz, M.; Schulze, H.; Lisdat, F.; Mount, A. R.; Bachmann, T. T. Alkaline Phosphatase Enzymatic Signal Amplification for Fast, Sensitive Impedimetric DNA Detection. *Analyst* **2012**, *137*, 59−63.
(18) Peng, Y.; Jiang, J.; Yu, R. A Sensitive Electrochemical Biosensor for MicroRNA Detection Based on Streptavidin−Gold Nanoparticles and Enzymatic Amplification. *Anal. Methods* **2014**, *6*, 2889−2893.
(19) Neves, M. P. S.; González-García, M. B.; Nouws, H. P.A.; Costa-Garcí, A. Celiac Disease Detection Using a Transglutaminase Electrochemical Immunosensor Fabricated on Nanohybrid Screen-printed Carbon Electrodes. *Biosens. Bioelectron.* **2012**, *31*, 95−100.
(20) Akanda, M. R.; Choe, Y. L.; Yang, H. Outer-Sphere to Inner-Sphere Redox Cycling for Ultrasensitive Immunosensors. *Anal. Chem.* **2012**, *84*, 1049−1055.
(21) Akanda, M. R.; Aziz, M. A.; Jo, K.; Tamilavan, V.; Hyun, M. H.; Kim, S.; Yang, H. Optimization of Phosphatase- and Redox Cycling-Based Immunosensors and Its Application to Ultrasensitive Detection of Troponin I. *Anal. Chem.* **2011**, *83*, 3926−3933.
(22) Yang, Z. H.; Zhuo, Y.; Yuan, R.; Chai, Y. Q. An Amplified Electrochemical Immunosensor based on in Situ-produced 1-Naphthol as Electroactive Substance and Graphene oxide and Pt Nanoparticles Functionalized CeO_2 Nanocomposites as Signal Enhancer. *Biosens. Bioelectron.* **2015**, *69*, 321−327.
(23) Kong, D. M.; Xu, J.; Shen, H. X. Positive Effects of ATP on G-Quadruplex-Hemin DNAzyme-Mediated Reactions. *Anal. Chem.* **2010**, *82*, 6148−6153.
(24) Zhou, M.; Kuralay, F.; Windmiller, J. R.; Wang, J. DNAzyme Logic-controlled Biofuel Cells for Self-powered Biosensors. *Chem. Commun.* **2012**, *48*, 3815−3817.
(25) Golub, E.; Freeman, R.; Willner, I. A Hemin/G-Quadruplex Acts as an NADH Oxidase and NADH Peroxidase Mimicking DNAzyme. *Angew. Chem., Int. Ed.* **2011**, *50*, 11710−11714.
(26) Zhang, M.; Xu, S.; Minteer, S. D.; Baum, D. A. Investigation of a Deoxyribozyme as a Biofuel Cell Catalyst. *J. Am. Chem. Soc.* **2011**, *133*, 15890−15893.
(27) Golub, E.; Freeman, R.; Willner, I. Hemin/G-Quadruplex-Catalyzed Aerobic Oxidation of Thiols to Disulfides: Application of the Process for the Development of Sensors and Aptasensors and for Probing Acetylcholine Esterase Activity. *Anal. Chem.* **2013**, *85*, 12126−12133.
(28) Willner, I.; Shlyahovsky, B.; Zayats, M.; Willner, B. DNAzymes for Sensing Nanobiotechnology and Logic Gate Applications. *Chem. Soc. Rev.* **2008**, *37*, 1153−1165.
(29) Yuan, Y.; Liu, G.; Yuan, R.; Chai, Y.; Gan, X.; Bai, L. Dendrimer Functionalized Reduced Graphene Oxide as Nanocarrier for Sensitive Pseudo Bienzyme Electroc Hemical Aptasens. *Biosens. Bioelectron.* **2013**, *42*, 474−480.
(30) Yi, H.; Xu, W.; Yuan, Y.; Bai, L.; Wu, Y.; Chai, Y.; Yuan, R. A Pseudo Triple-enzyme Cascade Amplified Aptasensor for Thrombin Detection based on Hemin/G-quadruplex as Signal Label. *Biosens. Bioelectron.* **2014**, *54*, 415−420.
(31) Yuan, Y.; Chai, Y.; Yuan, R.; Zhuo, Y.; Gan, X. An Ultrasensitive Electrochemical Aptasensor with Autonomous Assembly of Hemin−G-quadruplex DNAzyme Nanowires for Pseudo triple-enzyme Cascade Electrocatalytic Amplification. *Chem. Commun.* **2013**, *49*, 7328−7330.
(32) Motaung, D. E.; Mhlongo, G. H.; Nkosi, S. S.; Malgas, G. F.; Mwakikunga, B. W.; Coetsee, E.; Swart, H. C.; Abdallah, H. M. I.; Moyo, T.; Ray, S. S. Shape-Selective Dependence of Room Temperature Ferromagnetism Induced by Hierarchical ZnO Nanostructures. *ACS Appl. Mater. Interfaces* **2014**, *6*, 8981−8995.
(33) Park, S.; An, S.; Ko, H.; Jin, C.; Lee, C. Synthesis of Nanograined ZnO Nanowires and Their Enhanced Gas Sensing Properties. *ACS Appl. Mater. Interfaces* **2012**, *4*, 3650−3656.
(34) Li, N.; Jin, S. X.; Liao, Q. Y.; Wang, C. X. ZnO Anchored on Vertically Aligned Graphene: Binder-Free Anode Materials for Lithium-Ion Batteries. *ACS Appl. Mater. Interfaces* **2014**, *6*, 20590−20596.
(35) Wang, X.; Wang, W.; Liu, Y. L. Enhanced Acetone Sensing Performance of Au Nanoparticles Functionalized Flower-like ZnO. *Sens. Actuators B* **2012**, *168*, 39−45.
(36) Chen, L.; Luo, L.; Chen, Z.; Zhang, M.; Zapien, J. A.; Lee, C. S.; Lee, S. T. ZnO/Au Composite Nanoarrays as Substrates for Surface-enhanced Raman Scattering Detection. *J. Phys. Chem. C* **2010**, *114*, 93−100.
(37) Yan, Y.; Xiao, F. S.; Zheng, G.; Zhen, K.; Fang, C. Selective Catalytic Oxidation of Naphthol to 2-hydroxyl-1,4-naphthoquinone by Hydrogen Peroxide over Metalloporphyrin Catalysts. *J. Mol. Catal. A: Chem.* **2000**, *157*, 65−72.

DOI: 10.1021/acsami.5b00988
ACS Appl. Mater. Interfaces 2015, 7, 10308−10315